Journal of System Design and Dynamics

Vol. 1, No. 1, 2007

Reducing Floor Impact Vibration and Sound Using a Momentum Exchange Impact Damper*

Lovely SON**, Makoto KAWACHI**, Hiroshi MATSUHISA** and Hideo UTSUNO**

**Department of Precision Engineering, Kyoto University, Yoshidahonmachi, Sakyo-ku, Kyoto 606-8501, Japan

E-mail: lovelyson@std.mbox.media.kyoto-u.ac.jp

Abstract

This paper deals with reducing floor impact vibration and sound by using a momentum exchange impact damper. The impact damper consists of a spring and a mass that is contact with the floor. When a falling object collides with the floor, the floor interacts with the damper mass, and the momentum of the falling object is transferred to the damper. In this works a computational model is formulated to simulate dynamic floor vibration induced by impact. The floor vibration is simulated for various sized damper masses. A proof-of-concept experimental apparatus was fabricated to represent a floor with an impact damper. This example system consists of an acrylic plate, a ball for falling object, and an impact damper. A comparison between simulated and experimental results were in good agreement in suggesting that the proposed impact damper is effective at reducing floor impact vibration and sound by 25% and 63%, respectively.

Key words: Impact, Vibration Control, Flooring System, Momentum Exchange, Sound

1. Introduction

Floor vibration problems are common in many types of building structures. These vibrations can result from many sources (e.g., reciprocating machinery, explosions, and human activity). The human activities such as walking, dancing, jumping, etc have been reported as the most common problems. The forces resulting from these activities are particularly problem because they cannot be easily isolated from the structure and they occur frequently.

Many researches have been conducted to control floor vibrations. Early studies focused the research on the tuned mass dampers (TMDs). Allen and Pernica used TMDs consisting of wooden planks with weights on top for the reduction of annoying vibrations due to human walking [(1)]. Setareh and Hanson used TMDs to control the floor vibrations due to dancing in auditorium floor [(2)]. Webster and Vaicajtis used TMDs to control the annoying vibrations of a long-span cantilevered composite floor system due to human movements [(3)].

Recent years, research efforts on active control are increasingly used for reducing floor vibration. Hanagan and Murray used active control to reduce vibration level of floors [(4), (5)]. Even though active control has better performance than passive control, they have several disadvantages, such as needs for actuator, high operational costs, and high power requirements.

Here, a momentum exchange impact damper is used to control floor shock vibrations. The mechanism of impact dampers is described by considering the system shown in Fig. 1.

*Received 20 July, 2006 (No. 06-0073)
[DOI: 10.1299/jsdd.1.14]

A ball with mass m_b is hurled at floor that consist of a spring mass system with mass m and stiffness k. Mass m is in contact with the impact damper that consist of mass m_d, spring k_d and viscous damper c_d. At the instant after m_b collides with m, energy from m is continuously transferred to m_d by mean of momentum exchange.

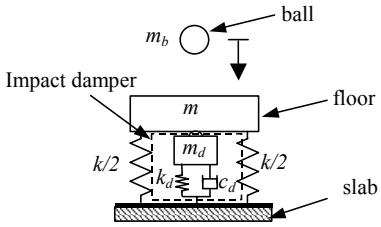

Fig. 1 Mechanism of impact damper

Nomenclature

$\mathbf{B_{fb}}$, $\mathbf{B_{fd}}$, $\mathbf{B_{sd}}$	vector defined in Eqs. (4), (5) and (6)
$\mathbf{C}$	damping matrix of the structure
c	speed of sound, m/s
c_{cb}	contact damping coefficient between ball and floor, Ns/m$^{3/2}$
c_d	damping coefficient of impact damper, Ns/m
d	diameter of steel ball, m
E_1	Young's modulus of acrylic plate, N/m^2
E_2	Young's modulus of steel ball, N/m^2
$e1$, $e2$, $e3$	the degree of freedom at the position of external forces f_{fb}, f_{fd} and f_{sd}
f_{fb}	contact force between floor and ball, N
f_{fd}	contact force between floor and impact damper, N
f_{sd}	transmitted force from impact damper to the slab, N
$\mathbf{K}$	stiffness matrix of the structure
k_{cb}	contact stiffness between ball and floor, N/m$^{3/2}$
k_{cd}	contact stiffness between impact damper and floor, N/m$^{3/2}$
k_d	stiffness of impact damper, N/m
L_x, L_y, L_z	dimension of rectangular room, m
$\mathbf{M}$	mass matrix of the structure
m_b	mass of ball, kg
m_d	mass of impact damper, kg
m_f	mass of floor, kg
N	the number of Fourier point
$NDOF$	the number of degree of freedom
n	The number of acoustic modes
p	sound pressure, Pa
q_i	modal displacement for ith mode
$q_{s,i}$	modal displacement of slab for ith mode
t_p	discrete time in Fourier transform
T_s	sampling time, s
u	displacement of the structure, m
u_f	displacement of floor at point O_f, m
u_s	displacement of slab at point O_s, m
v	velocity, m/s
v_s	normal velocity of slab, m/s
V_s	Fourier transform of normal velocity of slab

x, y, z	Cartesian coordinates
x_1	displacement of ball, m
x_2	displacement of impact damper, m

Greek symbols

β, β_n, β_q	acoustic damping factor
ϕ	velocity potential, m^2/s
Φ_n	velocity potential for n^{th} mode, m^2/s
ω_i	structure natural frequency for i^{th} mode, rad/s
ω_n, ω_q,	acoustic natural frequency
$\boldsymbol{\psi}_i$	mass normalized eigenvector for i^{th} mode
$\boldsymbol{\psi}_{s,i}(x,y)$	mass normalized eigenvector of slab for i^{th} mode
ζ_i	structure damping ratio for i^{th} mode

2. Flooring System with Impact Damper

In this work, an example flooring system consisting of floor (acrylic plate, $0.4\times 0.32\times 0.005$ m, $m_f = 0.75$ kg), support frame (steel), slab (concrete, $0.66\times 0.57\times 0.03$ m) and wooden box ($0.58\times 0.47\times 0.1$ m) for the room bellow the slab was analyzed (Fig. 2). The system has a novel impact damper placed between floor and a supporting slab. The impact damper is positioned in the center of the slab at O_s. The impact damper consists of a mass supported by spring and air damper ($k_d = 507$ N/m , $c_d = 40$ Ns/m). The damper was designed to have lower damping coefficient for forward motion than that for the return motion. The purpose of this technique is to allow fast movement during the moment at which the impact takes place. A steel ball ($d = 0.005$ m) is glued to the impact damper mass. The steel ball contacts the floor at point O_f which is located at the center of the floor. When the floor has an impact load, it will collide with the damper resulting in exchange of momentum between floor and damper. The impact force is generated by dropping a ball (tennis ball, $m_b = 0.054$ kg and acrylic ball $m_b = 0.045$ kg) from the height of 0.23 m onto point O_f. The contact surface between wooden box and the slab was shielded by resin foam. This foam was used to block the transmission wave via the gap between slab and wooden box.

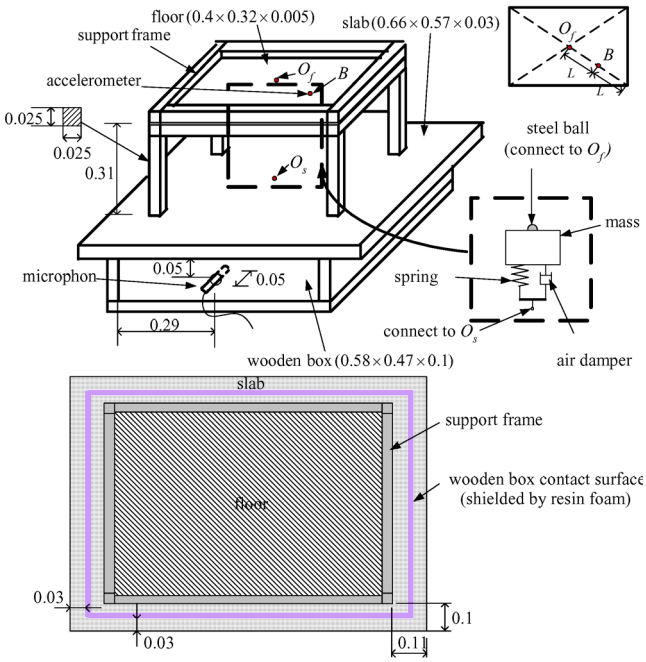

Fig. 2 Experimental apparatus of the flooring system with impact damper

3. Theoretical Model and Identification

Figure 3 shows the model of flooring system with momentum exchange impact damper. The governing equations for the structure consist of floor, support frame, slab and distributed linear spring are solved using Finite Element Method (FEM). Uniformly distributed linear springs are used to express the stiffness of resin foam located on the top contact surface of wooden box. Four-node quadrilateral plate elements were used to model both the floor and slab system. The support frame is modeled using three dimensional frame elements.

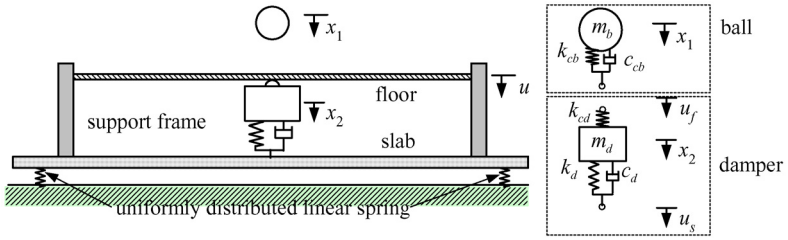

Fig. 3 Model of flooring system with impact damper

The equations of motion for the structure, ball, and impact damper are written as

$$\mathbf{M}\ddot{\mathbf{u}} + \mathbf{C}\dot{\mathbf{u}} + \mathbf{K}\mathbf{u} = \mathbf{B}_{\mathbf{fb}} f_{fb} - \mathbf{B}_{\mathbf{fd}} f_{fd} + \mathbf{B}_{\mathbf{sd}} f_{sd}, \tag{1}$$

$$m_b \ddot{x}_1 + f_{fb} = 0, \tag{2}$$

$$m_d \ddot{x}_2 + f_{sd} - f_{fd} = 0, \tag{3}$$

where matrix **M**, **C** and **K** are the structure mass matrix, damping matrix and stiffness matrix, respectively, while f_{fb}, f_{fd}, f_{sd}, m_b and m_d are the contact force between floor and ball, contact force between floor and impact damper, transmitted force from impact damper to slab, mass of ball and mass of impact damper, respectively. Vector **u**, x_1 and x_2 are displacement vector of the structure, displacement of ball and displacement of impact damper, respectively.

$\mathbf{B}_{\mathbf{fb}}$, $\mathbf{B}_{\mathbf{fd}}$ and $\mathbf{B}_{\mathbf{sd}}$ are vectors that depend on the position of external forces. These vectors can be expressed as,

$$\mathbf{B}_{\mathbf{fb}} = \left\{ \delta_{e1,1} \quad \delta_{e1,2} \cdots \delta_{e1,j} \cdots \quad \delta_{e1,NDOF} \right\}^{\mathrm{T}}, \tag{4}$$

$$\mathbf{B}_{\mathbf{fd}} = \left\{ \delta_{e2,1} \quad \delta_{e2,2} \cdots \delta_{e2,j} \cdots \quad \delta_{e2,NDOF} \right\}^{\mathrm{T}}, \tag{5}$$

$$\mathbf{B}_{\mathbf{sd}} = \left\{ \delta_{e3,1} \quad \delta_{e3,2} \cdots \delta_{e3,j} \cdots \quad \delta_{e3,NDOF} \right\}^{\mathrm{T}}, \tag{6}$$

where, $e1$, $e2$ and $e3$ denote the degree of freedom at the position of external forces f_{fb}, f_{fd} and f_{sd}, respectively, while $NDOF$ is the number of degree of freedom. $\delta_{i,j}$ is delta function which can be expressed as

$$\delta_{i,j} = \begin{cases} 1, i = j \\ 0, i \neq j \end{cases}. \tag{7}$$

Contact force between floor and ball was modeled using nonlinear spring and nonlinear dashpot [6]. Thus, the contact force can be expressed as

$$f_{fb} = \begin{cases} k_{cb}\left(x_1 - u_f\right)^{3/2} + c_{cb}\left|x_1 - u_f\right|^{1/2}\left(\dot{x}_1 - \dot{u}_f\right), & \left(x_1 - u_f\right) \geq 0 \\ 0, & \left(x_1 - u_f\right) < 0 \end{cases}, \tag{8}$$

where k_{cb} and c_{cb} are contact stiffness and contact damping coefficient between ball and

floor, respectively, while u_f is displacement of floor at point O_f.

Note that when the ball is in contact with the floor, the contact force affects the equation of motion and for out of contact case the equation of motion is not affected by contact force.

The transmitted force from impact damper to the slab can be expressed as

$$f_{sd} = c_d(\dot{x}_2 - \dot{u}_s) + k_d(x_2 - u_s), \tag{9}$$

where k_d and c_d are the stiffness and damping coefficient of impact damper, respectively, while variable u_s is displacement of slab at point O_s.

The impact damper damping coefficient for forward motion is very small and leads to

$$c_d = 0 \quad if \quad \dot{x}_2 - \dot{u}_s > 0 . \tag{10}$$

The contact force between floor and impact damper was modeled using Hertz contact theory [7]

$$f_{fd} = \begin{cases} k_{cd}\left(u_f - x_2\right)^{3/2}, & \left(u_f - x_2\right) \geq 0 \\ 0, & \left(u_f - x_2\right) < 0 \end{cases}, \tag{11}$$

where k_{cd} is contact stiffness between impact damper and floor.

Equation (1) can be written in modal coordinates giving

$$\ddot{q}_i + 2\zeta_i\omega_i\dot{q}_i + \omega_i^2 q_i = \boldsymbol{\psi}_i\left[\mathbf{B_{fb}}f_{fb} - \mathbf{B_{fd}}f_{fd} + \mathbf{B_{sd}}f_{sd}\right] \ , \mathrm{i} = 1,2,\cdots,\infty , \tag{12}$$

where q_i, ζ_i, ω_i, and $\boldsymbol{\psi}_i$ are the modal displacement, damping ratio, natural frequency and mass normalized eigenvector for ith mode, respectively.

The parameters k_{cb} and c_{cb} were determined by reconciling the simulation results and the experimental results for the contact force time response as shown in Table 1. The experimental results were obtained by dropping a ball from different initial heights on a small acrylic plate supported by a force sensor located in the center of the plate as shown in Fig. 4(a). Figure 4 (b) shows a comparison between the experimental and simulation result of tennis ball for h_0 = 0.15 m. It can be shown that there are good agreement between simulation and experimental result

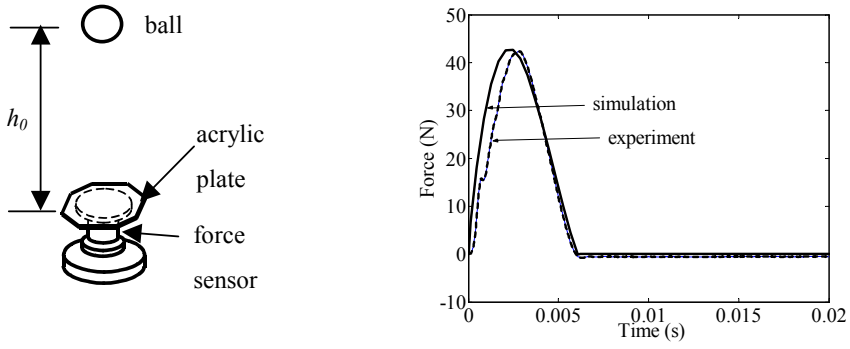

(a) (b)

Fig. 4 Determination of k_{cb} and c_{cb}

Table 1 Variation of k_{cb} and c_{cb}

h_0 (m)	Tennis ball		Acrylic ball	
	k_{cb} (N/m$^{3/2}$)	c_{cb} (Ns/m$^{3/2}$)	k_{cb} (N/m$^{3/2}$)	c_{cb} (Ns/m$^{3/2}$)
0.15	2.1×10^5	160	3.3×10^7	500
0.2	3.1×10^5	160	3.3×10^7	500
0.25	4.1×10^5	160	3.3×10^7	500

Figure 5 (a) ~ 5 (f) shows several low order mode shapes of the structure without damper obtained by FEM analysis. There are five important modes that play an important role for the center point response of the floor. The 4th mode, occurring at a 19.9 Hz frequency, is the first one. This mode is relating to rigid body motion of floor and slab in vertical direction. The other important modes are the 8th, 13th, 15th, and 18th corresponding to frequencies 151.1, 274.4, 347.1, and 448.3 Hz, respectively.

Figure 6 (a) and (b) show the comparison of Frequency Response Function (FRF) obtained from the simulation and experimental data. The experimental FRF was obtained by dividing the measured data of acceleration with input data of force in impulse test using impact hammer. Figure 6 (a) shows the results for the input point O_s and output point O_s. There are three dominant modes with frequencies about 19.9, 274.4, and 347.1 Hz. These frequencies relate to the 4th, 13th, and 15th modes, respectively. Figure 6 (b) shows the frequency response function for the input point B and output point B. It can be shown that the simulation model is good enough in expressing the dynamic characteristic of the structure. Based on these responses, seven damping ratios were identified: $\zeta_4 = 0.06$, $\zeta_8 = 0.018$, $\zeta_{12} = 0.019$, $\zeta_{13} = 0.010$, $\zeta_{14} = 0.022$, $\zeta_{15} = 0.01$, and $\zeta_{18} = 0.019$.

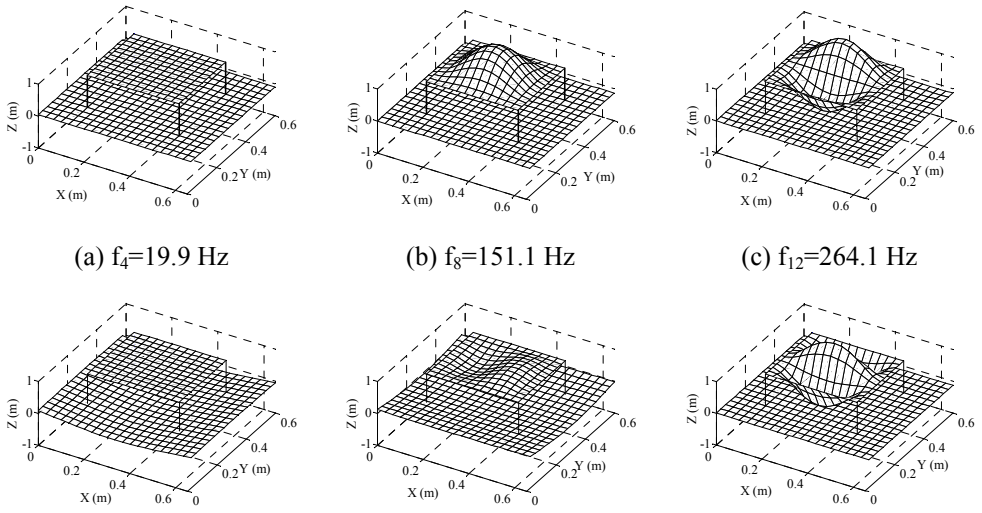

(a) f_4=19.9 Hz (b) f_8=151.1 Hz (c) f_{12}=264.1 Hz

(d) f_{13}=274.4 Hz (e) f_{15}=347.1 Hz (f) f_{18}=448.3 Hz

Fig. 5 Floor, support frame and slab mode shape

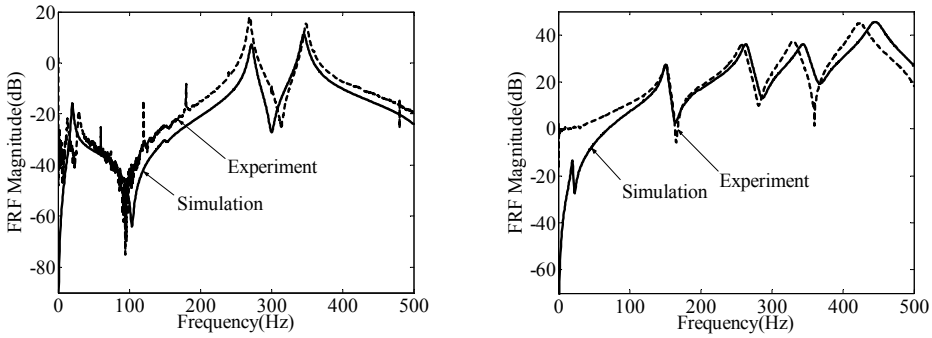

(a) input O_s, output O_s (b) input B, output B

Fig. 6 Frequency responses of floor and slab system

4. Sound Pressure Calculation

The transmitted forces from support frame and impact damper to the slab induce the vibration of the slab. According to the acoustic theory, the variation of velocity potential cause propagation of compressible wave inside the room below the slab as shown in Fig.7.

The wave equation governing the propagation of small disturbance through a

homogeneous and compressible fluid flow may be written in rectangular Cartesian coordinate as[8]

$$\frac{\partial^2\phi}{\partial t^2}=\left(\frac{c}{1+j\beta}\right)^2\left(\frac{\partial^2\phi}{\partial x^2}+\frac{\partial^2\phi}{\partial y^2}+\frac{\partial^2\phi}{\partial z^2}\right), \tag{13}$$

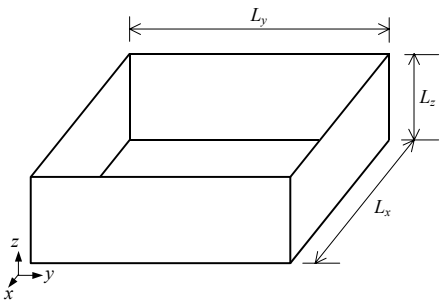

Fig. 7 The room bellow the slab

where β, ϕ, and c described the acoustic damping factor, velocity potential, and sound speed, respectively. It should be noted that the complex term of damping factor $j\beta$ was including in the wave equation to express the energy losses because of air reflection on the wall and air dispersion. The velocity potential ϕ is combination of several acoustic modes. Hence, it can be expressed as

$$\phi=\sum_n \Phi_n(x,y,z)e^{j\omega_n t}, \tag{14}$$

where ω_n is frequency. Φ_n in Eq. (14) can be expressed as multiplication of three partial functions $X_n(x)$, $Y_n(y)$, $Z_n(z)$ resulted

$$\phi=\sum_n X_n(x)Y_n(y)Z_n(z)e^{j\omega_n t}. \tag{15}$$

By considering the nth acoustic mode and introducing the velocity potential in Eq.(15) into wave equation in Eq.(13) yields

$$\frac{1}{X_n}\frac{d^2X_n}{dx^2}+\frac{1}{Y_n}\frac{d^2Y_n}{dy^2}+\frac{1}{Z_n}\frac{d^2Z_n}{dz^2}+\frac{\omega_n^2(1+j\beta_n)^2}{c^2}=0, \tag{16}$$

$$\mu_{x,n}^2+\mu_{y,n}^2+\mu_{z,n}^2=\frac{\omega_n^2(1+j\beta_n)^2}{c^2}, \tag{17}$$

where

$$\frac{d^2X_n}{dx^2}+\mu_{x,n}^2X_n=0, \tag{18}$$

$$\frac{d^2Y_n}{dy^2}+\mu_{y,n}^2Y_n=0, \tag{19}$$

$$\frac{d^2Z_n}{dz^2}+\mu_{z,n}^2Z_n=0. \tag{20}$$

Solution of Eqs.(18) ~ (20) is determined in the form

$$X_n=B_{1,n}\cos\mu_{x,n}x+B_{2,n}\sin\mu_{x,n}x, \tag{21}$$

$$Y_n=C_{1,n}\cos\mu_{y,n}y+C_{2,n}\sin\mu_{y,n}y, \tag{22}$$

$$Z_n=D_{1,n}\cos\mu_{z,n}z+D_{2,n}\sin\mu_{z,n}z. \tag{23}$$

The constants $B_{1,n}$, $B_{2,n}$, $C_{1,n}$, $C_{2,n}$, $D_{1,n}$, $D_{2,n}$ are determined by satisfying boundary conditions. The velocity field inside the room is relating to gradient of velocity potential as expressed in Eq. (24)

$$v(x,y,z,t)=-grad\,\phi=\left(-\frac{\partial\phi}{\partial x},-\frac{\partial\phi}{\partial y},-\frac{\partial\phi}{\partial z}\right). \tag{24}$$

Application of boundary conditions of rectangular room as shown in Fig.7 leads to

$$\frac{\partial\phi}{\partial x}=0 \quad \text{for} \quad x=0,\ L_x, \tag{25}$$

$$\frac{\partial \phi}{\partial y} = 0 \quad \text{for} \quad y = 0,\, L_y\,, \tag{26}$$

$$\frac{\partial \phi}{\partial z} = 0 \quad \text{for} \quad z = 0\,, \tag{27}$$

$$-\frac{\partial \phi}{\partial z}\bigg|_{z=Lz} = v_s\left(x,y,t\right), \tag{28}$$

where v_s is the normal velocity of the slab. The slab normal velocity can be expressed as

$$v_s\left(x,y,t\right) = \sum_{i=1}^{\infty} \boldsymbol{\psi}_{s,i}\left(x,y\right)\dot{q}_{s,i}\left(t\right), \tag{29}$$

where $\boldsymbol{\psi}_{s,i}\left(x,y\right)$, $\dot{q}_{s,i}\left(t\right)$ are eigenvector and modal velocity of the slab, respectively. Application of boundary conditions Eqs. (25) ~ (28) into Eqs. (21) ~ (23) yields

$$\Phi_n = \sum_{l=0}^{\infty}\sum_{m=0}^{\infty} A_{n(l,m)} \cos\frac{l\pi x}{L_x}\cos\frac{m\pi y}{L_y}\cos\mu_{n(l,m)}z\,, \tag{30}$$

where l,m are nonnegative integer. Substitution of Eq.(30) into Eq.(14) and applying the result into Eq.(28) leads to

$$\sum_{n}\sum_{l=0}^{\infty}\sum_{m=0}^{\infty} A_{n,(l,m)}\mu_{n,(l,m)} \cos\frac{l\pi x}{L_x}\cos\frac{m\pi y}{L_y}\sin\left\{\mu_{n,(l,m)}L_z\right\}e^{j\omega_n t} = v_s\left(x,y,z,t\right). \tag{31}$$

To obtain $A_{n,(l,m)}$, the summation term in equation in Eq.(31) should be simplified by introducing the inverse Fourier transform procedure

$$v_s\left(x,y,z,t_p\right) = \frac{2}{N}\sum_{q=0}^{N/2-1} V_s\left[x,y,\omega_q\right]e^{j\omega_q t_p}\,, \tag{32}$$

where V_s, N, t_p and ω_q are Fourier transform of v_s, the number of Fourier point, discrete time and discrete frequency in Fourier transform, respectively. The value of t_p and ω_q are determined in the form

$$t_p = pT_s\,, \tag{33}$$

$$\omega_q = \frac{2\pi q}{NT_s}\,, \tag{34}$$

where $q = 0,1,2,\ldots,N/2\text{-}1$, $p = 0,1,2,\ldots,N\text{-}1$ and T_s is sampling time.
Substitution of the result in Eq.(32) into Eq.(31) and by assuming the acoustic mode n is equal to q yields

$$\sum_{l=0}^{\infty}\sum_{m=0}^{\infty} A_{q,(l,m)}\mu_{q,(l,m)} \cos\frac{l\pi x}{L_x}\cos\frac{m\pi y}{L_y}\sin\left\{\mu_{q,(l,m)}L_z\right\} = \frac{2}{N}V_s\left(x,y,\omega_q\right). \tag{35}$$

It should be noted that the Fourier transform of $v_s(x,y,t_p)$ can be expressed as

$$V_s\left(x,y,\omega_q\right) = \sum_{p=0}^{N-1} v_s\left(x,y,t_p\right)e^{-j\omega_q t_p}\,. \tag{36}$$

Then, the expression in Eq.(29) and Eq.(36) is substituted into Eq.(35). Next, solution of $A_{q,(l,m)}$ is written in the form

$$A_{q,(l,m)} = \frac{\dfrac{2}{N}\displaystyle\sum_{i=1}^{\infty}\left[\sum_{p=0}^{N-1}\left\{\dot{q}_{s,i}\left(t_p\right)e^{-j\omega_q t_p}\iint_S \cos\frac{l\pi x}{L_x}\cos\frac{m\pi y}{L_y}\boldsymbol{\psi}_{s,i}\left(x,y\right)dS\right\}\right]}{\mu_{q,(l,m)}\sin\left\{\mu_{q,(l,m)}L_z\right\}\displaystyle\iint_S \cos^2\frac{l\pi x}{L_x}\cos^2\frac{m\pi y}{L_y}dS}, \tag{37}$$

and

$$\mu_{q,(l,m)} = \sqrt{\left\{\frac{\omega_q\left(1+j\beta_q\right)}{c}\right\}^2 - \left(\frac{l\pi}{L_x}\right)^2 - \left(\frac{m\pi}{L_y}\right)^2}\,, \tag{38}$$

where β_q and ω_q are acoustic damping factor, and acoustic natural frequency of the room, respectively. Integral operator $\iint_S \cdots dS$ in Eq.(37) is used to express the surface integral.

The velocity potential can be calculated as

$$\phi(x,y,z,t_p) = \sum_{q=0}^{N/2-1}\sum_{l=0}^{\infty}\sum_{m=0}^{\infty} A_{q,(l,m)} \cos\frac{l\pi x}{L_x}\cos\frac{m\pi y}{L_y}\cos\mu_{q,(l,m)} z e^{j\omega_q t_p} . \quad (39)$$

Finally, the sound pressure generated in the room bellow the slab can be expressed as

$$p = \rho_a \frac{\partial\phi}{\partial t}, \quad (40)$$

$$p(x,y,z,t_p) = \rho_a \sum_{q=0}^{N/2-1}\sum_{l=0}^{\infty}\sum_{m=0}^{\infty} j\omega_q A_{q,(l,m)} \cos\frac{l\pi x}{L_x}\cos\frac{m\pi y}{L_y}\cos\mu_{q,(l,m)} z e^{j\omega_q t_p}, \quad (41)$$

where ρ_a is density of air.

5. Simulation Result

The initial ball dropping height was 0.23 m. First, the low impact load was applied to the simulation system. The low impact load was realized by dropping a tennis ball (m_b = 0.054 kg) into the acrylic plate. The parameters k_{cb} and c_{cb} for tennis ball were interpolated from Table 1 giving values of 3.7×10^5 N/m$^{3/2}$ and 150 Ns/m$^{3/2}$, respectively. k_{cd} is taken as 6.1×10^8 Nm$^{-3/2}$ for contact radius $r_1 = \infty$ and r_2 = 0.005 m, Young's modulus E_1 = 5.9×10^9 N/m^2 for the acrylic flat contact, and E_2 = 210×10^9 N/m^2 for the steel spherical contact.

The sound pressure in the wooden box are calculated with the following constants: c = 340 m/s, ρ_a = 1.29 kg/m^3, β_q = 1.16 %. The acoustic damping factor was chosen to give comparable result with the experimental outcomes. In this case the acoustic damping factor was set such that the maximum peak for 4th mode in simulation result was almost the same as the peak spectrum obtained from experimental data.

Figure 8 shows the acceleration of floor at point B for three different cases. The first case is the response of the system without impact damper. The second and the third cases were the response of the system with mass ratios between impact damper and floor m_d/m_f of 0.6 and 1.2, respectively. In the simulation the floor mass m_f was set as 0.75 kg. The simulation results indicated that for mass ratios of 0.6 and 1.2 the maximum floor vibration could be reduced by 9% and 24%, respectively.

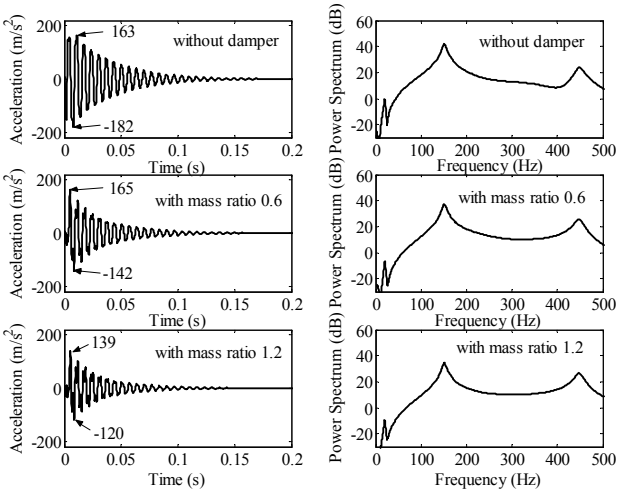

Fig. 8 Simulation results of acceleration in point B

Simulation results of sound pressure in the room bellow the slab is depicted in Fig. 9. The simulation results show that for mass ratios of 0.6 and 1.2, the sound pressure could be reduced by 53% and 67%, respectively. In the frequency response, the attenuations of sound power spectrum at the 8th mode for mass ratios of 0.6 and 1.2 are 4.6 and 7.7 dB, respectively.

It should be pointed out that the simulation results of floor acceleration response are

dominated by 8th mode with frequency 151.1 Hz but for the sound pressure response, the 4th mode with frequency 19.9 Hz has the major contribution to the total response.

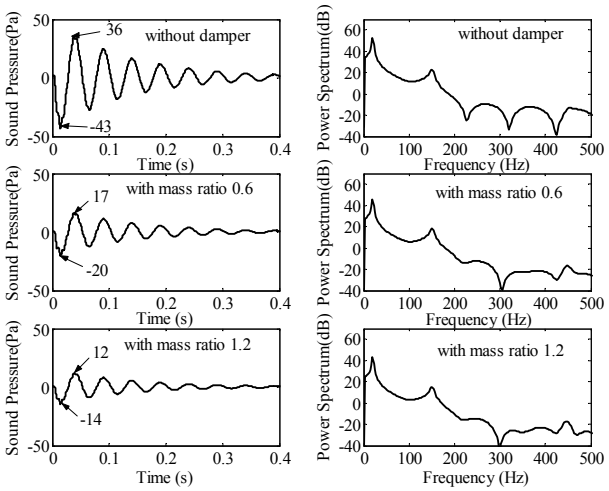

Fig. 9 Simulation results sound pressure in the wooden box

The vibration suppression obtained by using impact damper is compared to conventional added mass method for high impact load case. The high impact load was obtained by dropping a mass with high contact stiffness to the floor. The mass tip was made from acrylic ball (m_b = 0.045 kg). The contact stiffness between floor and acrylic ball was obtained from Table 1. Three-simulation procedure was conducted. First, the response is calculated for case without damper. The second case is calculation using added mass 0.3 kg located in the center of the floor. The third case is calculation using impact damper with mass ratio 0.4(m_d = 0.3 kg). The impact damper was used to suppress the low frequency vibration response excited by impact force. For this reason the low pass filter within 1 kHz frequency was used in the analysis.

Figure 10 shows the comparison of floor acceleration in point B without damper, with impact damper and with added mass cases, respectively. It can be shown from Fig.10 that the impact damper has superior performance in suppressing 8th mode (151.1 Hz) and 18th mode (448.3 Hz) compare to added mass method.

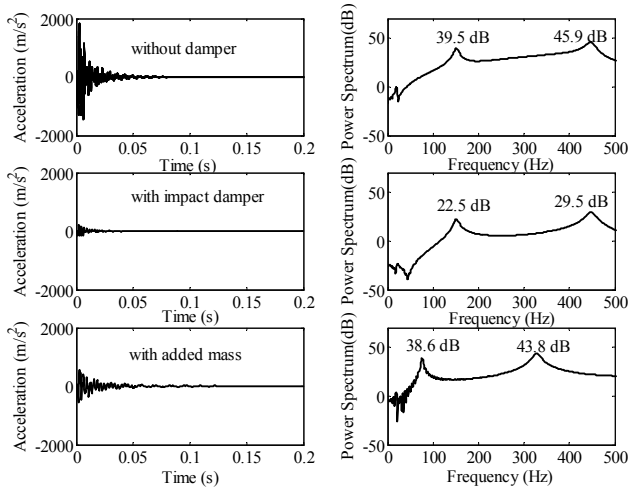

Fig.10 Simulation results comparison of acceleration response

Figure 11 shows the simulation results of sound pressure generation in the room bellow the slab for high impact load case. As the soft impact case, the sound pressure response is dominated by rigid body mode. It can be shown from Fig.11 that the attenuation of sound pressure using impact damper is higher than the conventional added mass method.

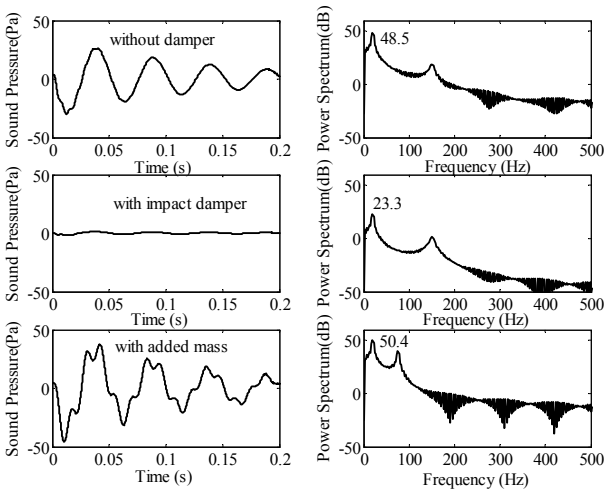

Fig. 11 Simulation results comparison of sound pressure

6. Experimental Result

The simulation result of floor acceleration and sound pressure generation in the room bellow the slab was tested experimentally. Experimental results for the case of low impact load using tennis ball are shown in Fig. 12 and Fig.13. Figure 12 shows that the maximum acceleration is reduced by 10 % and 25% by using the impact damper with mass ratios 0.6 and 1.2, respectively. There are two peaks appear between 150 Hz and 400 Hz which are not detected in simulation result. These peaks may be resulted from non-center collision between ball and floor.

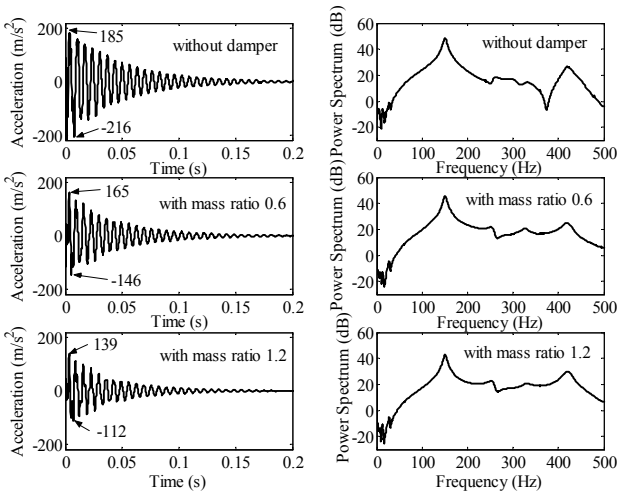

Fig. 12 Experimental results of acceleration in point B

The sound pressure response in the hypothetical room bellow the slab is shown in Fig. 13. Sound pressure is reduced by 50% and 63 % by the damper for mass ratios 0.6 and 1.2, respectively. Frequency response in Fig. 13 shows that the attenuations of sound power spectrum at the 8th mode for mass ratios of 0.6 and 1.2 are 2.55 and 2.79 dB, respectively.

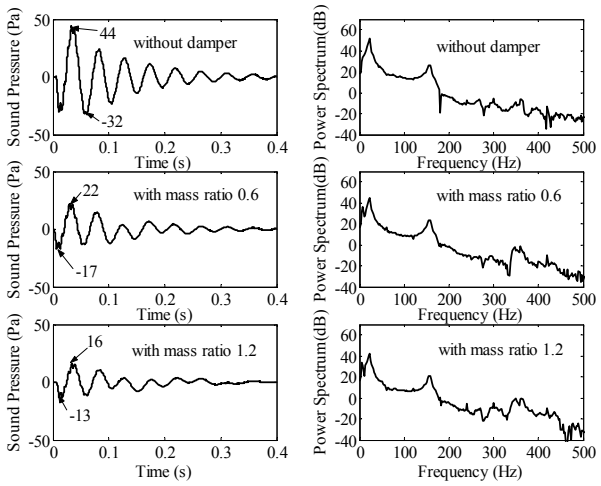

Fig. 13 Experimental results sound pressure in the wooden box

Experimental results of floor acceleration for high impact load are depicted in Fig. 14. Figure 14 shows that the vibration suppression obtained by using impact damper for 8th mode was better than that of added mass case. The resonance peaks for this mode are 24.2 dB and 28.3 dB for impact damper case and added mass case, respectively. The resonance peak of 18th mode using impact damper is 31.4 dB. This value is lower than added mass case 32.8 dB.

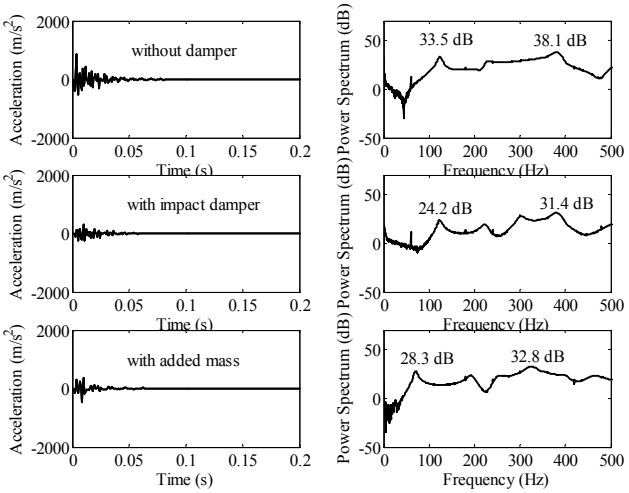

Fig. 14 Experimental results comparison of acceleration response

Figure 15 shows the experimental results of sound pressure generation for high impact load. The sound pressure response is dominated by rigid body mode. The resonance peak of rigid body mode using impact damper and added mass method are 17.5 dB and 30.7dB, respectively. These results show that the attenuation of sound pressure generation using impact damper method is higher than that of the added mass method.

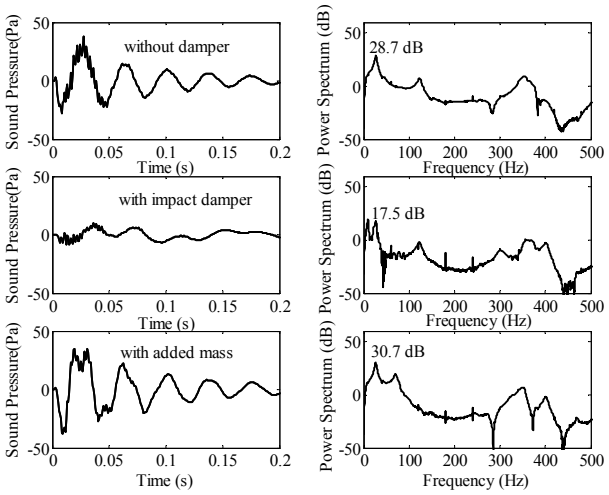

Fig. 15 Experimental results comparison of sound pressure

7. Conclusions

In the present research, a new impact damper device has been invented to absorb floor vibration and to suppress the resulting sound pressure level generated by a flooring system. A numerical model of flooring system was generated using a FEM formulation. The model was order-reduced by using modal analysis. A small-scale model of flooring system was then fabricated to show the effectiveness of impact damper in reducing the impact vibration. Finally, the experimental results were compared to the model simulation results. The maximum floor impact vibration and sound generation depended strongly on the impact damper mass ratio. The experimental results show that for a mass ratio of 1.2, the acceleration of the floor and sound pressure generated could be reduced by 25% and 63%, respectively.

Comparison of impact damper method to conventional added mass at the center of the floor was conducted for case of high impact load. The results show that impact damper has the better performance compare to added mass method in suppressing the floor acceleration and sound pressure generation.

References

(1) Allen, D.E., and Pernica, G., A simple absorber for walking vibrations, *Canadian Journal of Civil Engineering*, Vol. 11(1984), pp.112-117.
(2) Setareh, M., and Hanson, R.D., Tuned mass dampers to control floor vibrations from humans, *ASCE Journal of Structural Engineering*, Vol. 118(1992), pp.741-762.
(3) Webster, A.C., and Vaicajtis, R., Application of tuned mass dampers to control vibrations of composite-floor systems, *Engineering Journal of the American Institute of Steel Construction*, Vol. 29(1992), pp. 116-124.
(4) Hanagan, L.M., and Murray, T.M., Experimental results from the active control of floor motion. *Proceedings of the first world conference on structural control*, Pasadena, Calif., Vol. 3(1994), pp. FP4-71-FP4-78.
(5) Hanagan, L.M., and Murray, T.M., Active control approach for reducing floor vibrations, *ASCE Journal of Structural Engineering*, Vol. 123(1997), pp.1497-1505.
(6) Hongo, T., Sato, H., Iwata, Y., Komatsuzaki, T., and Hongo, Y., Modeling and Analysis of Impact Syatem Composed of Ball and Plane, *J.Jpn.Soc.Mech.Eng.*,(in Japanese), Vol.65, No.634, C(1999), pp.2287-2293.
(7) Love, A.E.H., *A Treatise on the Mathematical Theory of Elasticity* (Dover, New York), 4th ed. (1944), pp.193-200.
(8) Craggi, A., A Finite element Model for Acoustically Lined Small Rooms, J. *Sound and Vibration*. 108(1986), pp. 327-337